Structural, Electronic, Elastic, and Optical Properties of Cubic $BaLiX_3$ (X = F, Cl, Br, or I) Perovskites: An *Ab-initio* DFT Study

Redi Kristian Pingak[1*], Soukaina Bouhmaidi[2], Larbi Setti[2], Bartholomeus Pasangka[1], Bernandus Bernandus[1], Hadi Imam Sutaji[1], Fidelis Nitti[3], and Meksianis Zadrak Ndii[4]

[1]*Department of Physics, Faculty of Science and Engineering, Universitas Nusa Cendana, Jl. Adisucipto Penfui, Kupang 85001, Nusa Tenggara Timur, Indonesia*

[2]*Laboratory of Advanced Science and Technologies, FPL, Abdelmalek Essaadi University, Tetouan 93030, Morocco*

[3]*Department of Chemistry, Faculty of Science and Engineering, Universitas Nusa Cendana, Jl. Adisucipto Penfui, Kupang 85001, Nusa Tenggara Timur, Indonesia*

[4]*Department of Mathematics, Faculty of Science and Engineering, Universitas Nusa Cendana, Jl. Adisucipto Penfui, Kupang 85001, Nusa Tenggara Timur, Indonesia*

* ***Corresponding author:***

email: rpingak@staf.undana.ac.id

Received: March 19, 2023
Accepted: May 8, 2023

DOI: 10.22146/ijc.83261

Abstract: *This study reports for the first time the theoretical prediction of structural, electronic, elastic and optical properties of cubic $BaLiCl_3$, $BaLiBr_3$, and $BaLiI_3$ perovskites. The corresponding properties of the well-known $BaLiF_3$ are also theoretically investigated. Density Functional Theory (DFT) using the Generalized Gradient Approximation (GGA) was implemented within the Quantum Espresso package to investigate the properties of the perovskites. The results revealed that $BaLiX_3$ (X = F, Cl, Br, and I) are in ionic crystal forms with optimized lattice parameters of 4.04, 4.90, 5.21, and 5.66 Å, respectively. The minor band gaps were found to be 6.62 eV (Γ→Γ), 4.29 eV (R→Γ), 3.50 eV (R→Γ), and 2.58 eV (R→Γ) for the respective compounds. The investigation of their elastic properties indicated that these perovskites are all mechanically stable, while only $BaLiBr_3$ and $BaLiI_3$ are malleable. Finally, the studied perovskites exhibit excellent optical properties, including low reflectivity and high absorption in the ultraviolet region. Hence, it is predicted that these perovskites are suitable for various optoelectronic applications involving absorption in the UV region. However, $BaLiBr_3$ and $BaLiI_3$ are more favorable than $BaLiF_3$ and $BaLiCl_3$ to be deposited as thin films due to their flexibility.*

Keywords: *Density Functional Theory; Quantum Espresso; $BaLiX_3$ perovskites; elastic properties; optoelectronic properties*

■ INTRODUCTION

Perovskites ABX_3, where A and B are two cations, and X is an anion, can be formed by an arrangement of many possible atoms. This is because most of the elements in the periodic table can replace elements in the A and B sites. In a unit cell, the B-site cation occupies the center of the octahedron and is coordinated by six X anions, whereas the top corner of the cube is occupied by A cations [1].

Due to its enormous number of structural families with specific properties, the ABX_3 perovskites have found substantial roles in various potential applications. This fact has therefore garnered significant attention and thus attracted a considerable amount of research conducted on the ABX_3 perovskites by the scientific community. For example, hybrid organic-inorganic perovskites have been widely applied in optoelectronic devices, including solar cells, due to their tunable electronic properties [2-7]. Because of their low cost and easily-tailored structure, the perovskites can be specifically designed and applied in catalysts and thermoelectric devices [8-9].

$BaLiF_3$, in particular, has been intensively investigated in some recent studies due to its potential application in various fields, including dosimetry and computed radiography. The first theoretical study on the physical properties of cubic $BaLiF_3$ (space group $pm\bar{3}m$) was presented by Korba et al. [10], which was in good agreement with previously reported experimental results by Boumriche et al. [11]. In addition, Düvel and co-workers [12] successfully synthesized a highly pure $BaLiF_3$ nanocrystal with this cubic perovskite structure, further verifying the theoretical prediction presented in [10]. Since then, there have been several studies conducted to investigate further these perovskites, which covered not only the theoretical and computational aspects [13-17] but also the experimental point of view [18].

A literature study indicated that the above-mentioned computational studies revealed that $BaLiF_3$ perovskite possesses quite a flat band diagram. This is crucial as materials with flat band energy diagrams are highly likely to have strong anharmonicity and excellent thermoelectric properties [19-20]. Indeed, Song and co-workers [19] confirmed the flat band diagrams of some Thallium-based fluoro perovskites reported in our previous work [21]. They further confirmed that these types of perovskites have strong anharmonicity and high thermoelectric performance. This finding strongly suggests that $BaLiF_3$ and its isoelectronic compounds might have other applications as thermoelectric materials due to the overall flat band diagram of $BaLiF_3$.

Although the properties of $BaLiF_3$ have been intensively investigated, those of their isoelectronic, including $BaLiCl_3$, $BaLiBr_3$, and $BaLiI_3$, have not been fully addressed. Due to its accuracy, Density Functional Theory (DFT) has long been used to accurately predict the properties of a wide range of materials, some of which can be found in several recent studies reported in Refs [22-30]. Therefore, the present work aims to conduct a DFT study to investigate the structural, electronic, elastic and optical properties of cubic $BaLiX_3$ (X = F, Cl, Br, or I) perovskites. The results of this study are expected to pave the way to the understanding of their physical properties and potential applications in various devices.

■ COMPUTATIONAL DETAILS

Using the Quantum Espresso (QE) code [31], the DFT calculation with Generalized Gradient Approximation Perdew-Burke-Ernzerhof (GGA-PBE) functional [32] was conducted to investigate the structural, electronic, optical and elastic properties of cubic $BaLiX_3$ (X = F, Cl, Br, or I) perovskites. The ultrasoft pseudopotential was used to consider the interaction between electrons and nuclei of the constituent atoms in the materials. The structure was optimized using Broyden Fletcher-Goldfarb-Shanno (BFGS) minimization procedure. Furthermore, the thermo_pw program, which uses Quantum Espresso as the underlying engine, was used to calculate the optical and elastic properties of the perovskites. The Quantum Espresso code has recently been applied to accurately predict the properties of a wide range of materials [33-35].

The wave function and the charge density energy cut-offs were 40 Ry and 400 Ry, respectively. K-points of $5 \times 5 \times 5$ and $12 \times 12 \times 12$ were used for Self-Consistent Field (SCF) and Non-Self-Consistent Field (NSCF) calculation, respectively. The convergence threshold for the total energy was 10^{-8} Ry.

■ RESULTS AND DISCUSSION

Structural Properties

The cubic structure of $BaLiX_3$ (X = F, Cl, Br, or I) perovskites has space group #221 ($pm\bar{3}m$). Fig. 1 shows the unit cell structure of the perovskites, where Ba cations are located at Wyckoff coordinates of (0, 0, 0), and Li is at (0.5, 0.5, 0.5). Meanwhile, the three X anions are located at (0.5, 0, 0.5), (0.5, 0.5, 0) and (0, 0.5, 0.5).

The total energy of the compounds was calculated as a function of the lattice constants, as illustrated in Fig. 2. Cell relaxation was then performed to optimize the cubic structure of $BaLiX_3$ (X = F, Cl, Br, or I) perovskites, using the Birch-Murnaghan equation of states [36-38], as shown in Eq. (1).

$$E(V) = E_0 + \frac{B}{B'(B'-1)}\left[V\left(\frac{V_0}{V}\right)^{B'} - V_0\right] + \frac{B}{B'(V-V_0)} \quad (1)$$

Computed optimized lattice parameters of the materials are depicted in Table 1, whereas other computed structural parameters are shown in Table 2.

Table 1 shows that the optimized lattice constant of $BaLiF_3$ obtained in this study strongly agrees with the corresponding value obtained by Refs [10,12,15-16,39] using the GGA functional and is only slightly larger than the experimental value [11]. This step illustrates the reliability of our calculation, which should apply to other compounds studied in this work. Meanwhile, the optimized lattice parameters of $BaLiCl_3$, $BaLiBr_3$, and $BaLiI_3$ are reported for the first time in the present study and, therefore, can be used as a reference for further studies on these compounds.

It can also be seen from Table 1 that there is an increase in the optimized lattice constants of the compounds as Cl, Br, and I substitute F. This is due to the increase in the ionic radii when tuning the halide ions. This fact was also actual for other ABX_3 (X = F, Cl, Br, or I) perovskites ranging from lead-based halide perovskites [41-44] to lead-free perovskites including Ge-based compounds [45-49], Sn-based compounds [50-53], and other lead-free perovskite materials [54-59]. Indeed, this is also verified by experimental studies.

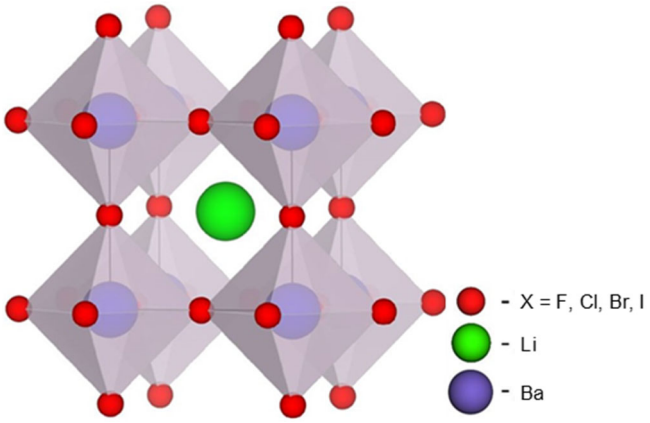

Fig 1. The unit cell structure of the cubic $BaLiX_3$ (X = F, Cl, Br, or I) perovskites

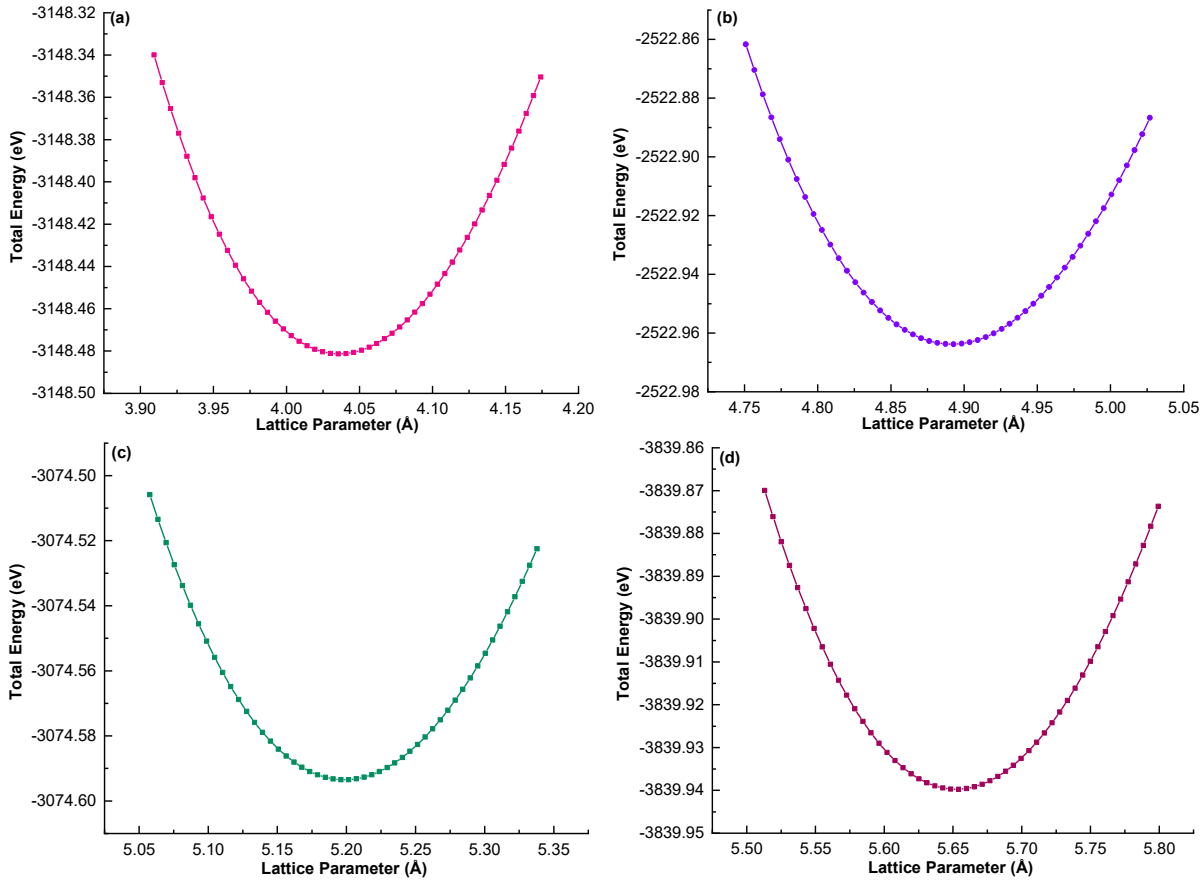

Fig 2. Total energy vs. lattice parameters of $BaLiF_3$ (a), $BaLiCl_3$ (b), $BaLiBr_3$ (c), and $BaLiI_3$ (d) perovskites

Table 1. Optimized lattice parameters and energy gaps of cubic $BaLiX_3$ (X = F, Cl, Br, or I) perovskites using the GGA functional

Compounds	Optimized lattice parameters (Å)		Energy gap (eV)	
	This work	Literature	This work	Literature
$BaLiF_3$	4.04	**GGA**: 4.05 [10]; 4.04 [12]; 4.04 [15]; 4.04 [16]; 4.03 [39] **Exp.**: 3.996 [11]	**6.62 (Γ→Γ)** 6.73 (R→Γ) 6.77 (M→Γ) 7.03 (X→Γ)	**GGA** (Γ→Γ): 6.66 [10]; 6.8 [15]; 6.72 [16] **Exp.** (Γ→Γ): 9.8 [40]
$BaLiCl_3$	4.90	-	4.37 (Γ→Γ) **4.29 (R→Γ)** 4.36 (M→Γ) 4.74 (X→Γ)	-
$BaLiBr_3$	5.21	-	3.62 (Γ→Γ) **3.50 (R→Γ)** 3.57 (M→Γ) 4.00 (X→Γ)	-
$BaLiI_3$	5.66	-	2.77 (Γ→Γ) **2.58 (R→Γ)** 2.67 (M→Γ) 3.15 (X→Γ)	-

Table 2. Structural parameters of cubic $BaLiX_3$ (X = F, Cl, Br, or I) using the GGA functional

Compound	V (a.u)^3	B (GPa)	B'	E_0 (Ry)	Total mass (a.m.u.)	Density (g/cm^3)
$BaLiF_3$	466.52021	67.90	4.69	-231.409	201.2632	5.049
$BaLiCl_3$	795.00231	33.86	4.54	-185.434	250.6180	3.530
$BaLiBr_3$	954.66886	27.14	4.53	-225.978	383.9680	4.505
$BaLiI_3$	1227.40669	20.67	4.25	-282.230	524.9800	4.791

For instance, the experimental value of the lattice parameter of $CsPbCl_3$ is 5.61 Å [60], slightly lower than that of $CsPbBr_3$ (5.87 Å) [43] and $CsPbI_3$ (6.29 Å) [61]. This verification by the experimental studies implies the accuracy of the DFT calculation.

Other computed structural parameters of the $BaLiX_3$ (X = F, Cl, Br, or I) perovskites, including their volume (V), bulk modulus (B), pressure derivative (B'), total energy (E_0), total mass and density are depicted in Table 2.

The computed value of the bulk modulus (B) of $BaLiF_3$ in this study (67.90 GPa) as a result of fitting Eq. (1), as shown in Table 2, is in excellent agreement with a value of 64.45 GPa [10], 66.46 GPa [14], and 65.7 GPa [15]. Likewise, the derivative of the bulk modulus concerning pressure (B') obtained in this study (4.69) is approximately the same as that reported by Korba et al. [10] (4.60), Mubarak and Mousa [14] (5.17), and Mousa et al. [15] (5.20). The other structural properties in Table 2, especially those of $BaLiCl_3$, $BaLiBr_3$, and $BaLiI_3$ perovskites, are presented for the first time in this study.

The formation energy ΔE_f of the compounds has been calculated using Eq. (2) to investigate the chemical and thermodynamic stability of the perovskites.

$$\Delta E_f = \frac{E_{tot}(BaLiX_3) - E(Ba) - E(Li) - 3E(X)}{N} \quad (2)$$

where E_{tot} ($BaLiX_3$) is the unit cell total energy of the $BaLiX_3$ perovskites, E(Ba), E(Li), and E(X) are the energy of Ba, Li, and X (X = F, Cl, Br, or I) atoms, respectively, and N is the number of atoms in the unit cell. The calculated values of the formation energy are −3.96, −3.21, −2.27, and −1.60 eV/atom for $BaLiF_3$, $BaLiCl_3$,

$BaLiBr_3$, and $BaLiI_3$, respectively. The negative values of the formation energy of all the studied perovskites indicate that they are thermodynamically and chemically stable and, therefore, can be experimentally synthesized. $BaLiF_3$ has been experimentally observed [11,40]. By assessing the formation energy of the compounds, we observe that the substitution of F with Cl, Br, or I increases the formation energy. This finding indicates a slight reduction in the chemical stability of the compounds following the halogen replacement. This decrease can be partly attributed to the decrease in the ionic character of the compounds, as the order of the halogen replacement was from F to I, as discussed in the following section.

Electronic Properties

The optimized lattice parameters obtained were then used to calculate other properties of the compounds, including the electronic properties. In this section, the electronic properties: Density of States (DOS), band diagram and charge density are presented and discussed.

The energy band diagrams and the total density of states of the compounds are plotted in Fig. 3, whereas the values of their band gap energies are summarized in Table 1. From columns 4 and 5 of Table 1, it is evident that the band gap of $BaLiF_3$ obtained in the present work agrees with that obtained using the GGA functional reported in [10,15-16]. It is also worth noting that the experimental band gap is underestimated in the present study and those using the GGA, as expected.

Table 1 also reveals that the band gap of the materials is tuned to lower values as Cl, Br, and I replace F. This is generally true for ABX_3 perovskites. Moreover, some recent studies also reported the same phenomenon for double perovskites of the form of $A_2B'B''X_6$ (X = Cl, Br, or I), such as Rb_2SnX_6 [62], Cs_2InBiX_6 [63-64], Cs_2AgCrX_6 [65], Rb_2AlInX_6 [66], Cs_2KTlX_6 [67],

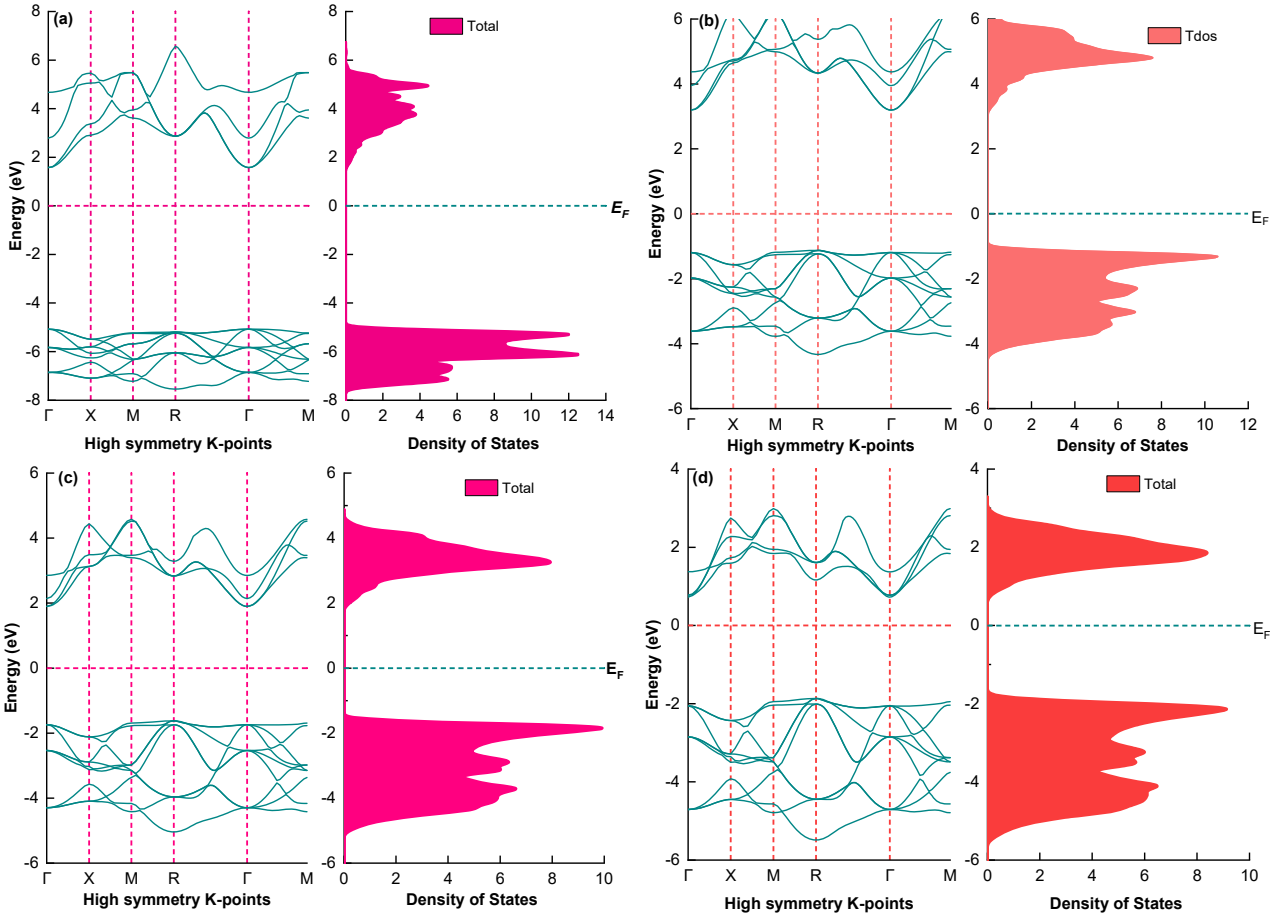

Fig 3. Energy band diagram and DOS of the cubic $BaLiF_3$ (a), $BaLiCl_3$ (b), $BaLiBr_3$ (c), and $BaLiI_3$ (d) perovskites

Cs_2AgBiX_6 [68], K_2ScAgX_6 [69], $(CsMA)NaSbX_6$ [70], Cs_2ScAgX_6 [71], Cs_2NaBiX_6 [72], Rb_2InBiX_6 [73], and Rb_2AgInX_6 [74]. Some new double perovskites of the form A_2BX_6 (X = Cl, Br, or I) also possess the corresponding tunable energy gap due to changing halogens. These include Cs_2PtX_6 [75], Ga_2TiX_6 [76], Cs_2PdX_6 [77], Tl_2PtX_6 [78], Cs_2TeX_6 [79], and Tl_2TiX_6 [80].

It is important to note that when F is replaced by Cl, Br, or I in $BaLiX_3$, the lattice parameters of the compounds are inversely proportional to their band gap energies (Table 1). As seen from Table 1, the lattice constants of the compounds increase while their energy gaps decrease with the ion replacement. This fact is due to the increase in the bond length of the compound following the increase in its lattice parameter, which causes the valence electrons within the compounds to be less bound to their parent atoms. Therefore, less energy is required to move them freely as conduction electrons, decreasing the compounds' energy gap. This phenomenon has also been observed in many other perovskites and double perovskites, in which the halide ion is substituted by its counterparts [41-59,62-80].

In ionic solids, electrons are firmly bound to their parents' atoms, and therefore relatively large energy is required to excite them to the conduction bands of the compounds. Consequently, ionic compounds tend to have significant band gap energy. In the case of the present study, the corresponding compounds have significant band gap energy, more significant than 2.5 eV, when using the GGA functional. Moreover, as the ionic character of the compounds decreases when F is replaced by Cl, Br, or I (Fig. 4), the band energy of the compounds is expected to decrease, as confirmed by our results. This finding demonstrates that the decrease in the ionic characters causes the valence electrons to be less bound to the nuclei, requiring less energy to be excited to the conduction band.

The general feature of the band diagram and the density of states of $BaLiF_3$ (as shown in Fig. 3(a)) is in excellent agreement with that reported in Refs [10,13-17]. The band diagrams and the density of states of $BaLiCl_3$, $BaLiBr_3$, and $BaLiI_3$ perovskites, on the other hand, are studied for the first time in the present work, where the smallest band gap energies of the compounds are found to be indirect: 4.29 eV (R→Γ), 3.5 eV (R→Γ), and 2.58 eV (R→Γ), for the respective compounds. The smallest band gap energies of the compounds are in bold in Table 1, where band gap energies of (Γ→Γ), (M→Γ), and (X→Γ) are also presented for comparison.

Furthermore, Fig. 3 clearly illustrates that the materials have relatively flat band gaps, especially valence bands. This is a unique and interesting property that might lead to potential applications in other devices, including thermoelectric devices [19-20]. More importantly, the coexistence of the flat band gaps and the high dispersion in the band structure contributes to the immense power factor (PF), as the former provides a larger thermopower (S). In contrast, the latter provides a higher electrical conductivity (σ) [19]. As seen in Fig. 3, the flat bands are observed in the valence bands of the compounds along M, R, and Γ high symmetry points. Further investigation on the thermoelectric properties of these materials is therefore highly recommended, with $BaLiI_3$ predicted to have better thermoelectric properties due to its smaller band gap than the other 3 materials. The material will be more suitable for thermoelectric materials by tuning further its band gap to a lower value, such as by applying external pressure.

To investigate chemical bonds present within the perovskites, their electron density in the (110) and (100) planes is illustrated in Fig. 4. Fig. 4(a) and 4(b) clearly show that the Ba-F and Li-F bonds within $BaLiF_3$ are primarily ionic, as seen from nearly spherical electronic distribution around the corresponding atoms. This finding can be further verified using Eq. (3) [81].

$$\%IC = \left[1 - e^{-0.25(X_1 - X_2)^2}\right] \times 100 \quad (3)$$

where IC stands for Ionic Character while X_1 and X_2 are the electronegativities of atom 1 and atom 2, respectively. Using Eq. (3), % ionic character values for Ba-F and Li-F bonds are 90.81 and 89.46%, respectively. This finding is consistent with the analysis reported by Lv et al. [17].

Furthermore, the present study reveals that the strength of the Li-X ionic bonds decreases as F is

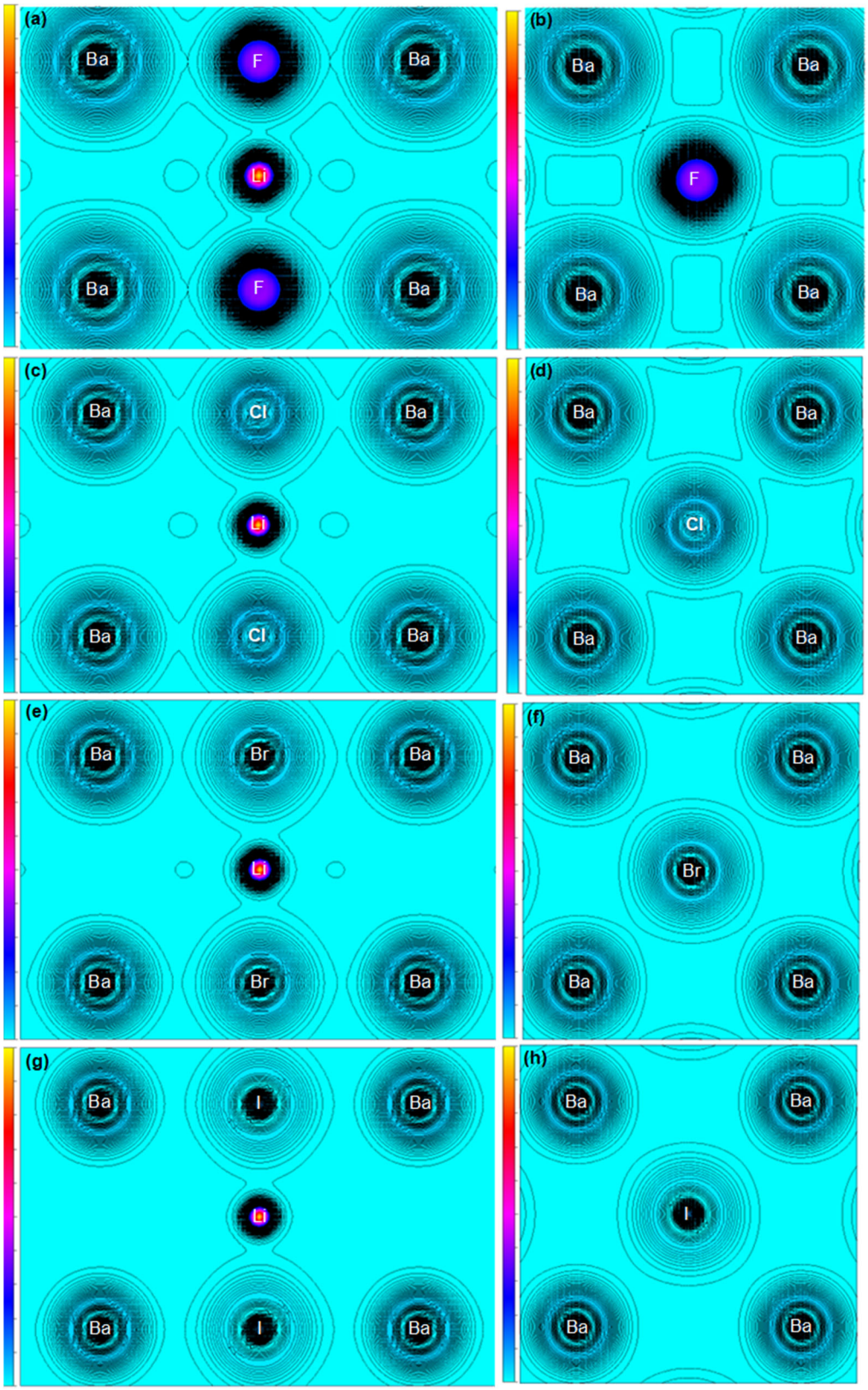

Fig 4. (110) Electron density of $BaLiF_3$ (a), $BaLiCl_3$ (c), $BaLiBr_3$ (e) and $BaLiI_3$ (g) and (100) electron density of $BaLiF_3$ (b), $BaLiCl_3$ (d), $BaLiBr_3$ (f) and $BaLiI_3$ (h)

substituted by Cl, Br, or I. This can be clearly seen from their electron charge density in the (110) plane as presented in Fig. 4(a, c, e and g), where electron distribution around X anions becomes more distorted as F is substituted by Cl, Br, or I, respectively. The distortion results in the charge density being less spherical, which implies a decrease in the ionic character of Li-X bonds for the ion replacement. This finding is attributed to the fact that the ions are of different sizes, with I^- the largest anion, followed by Br^-, Cl^-, and F^-. Larger X^- anions will be more electrically polarized in the presence of the Li^+ ion, and therefore their charge distribution will be less spherical, resulting in more electrons being more localized in the regions between Li-X. This is an indication that the covalent character of the Li-X bonds increases as X becomes more prominent in size. In other words, the ionic character of Li-X decreases due to the substitution of X with larger anions. Despite the decrease in the ionic character, the Li-X (X = F, Cl, Br, and I) bonds are still mainly ionic and partly covalent. This character can be verified using Eq. (3), from which the ionic character percentages of Li-F, Li-Cl, Li-Br, and Li-I bonds are 89.46, 69.52, 62.47, and 50.62%, respectively.

To see the character of Ba-X bonds more clearly, the electron density of the cubic $BaLiF_3$, $BaLiCl_3$, $BaLiBr_3$, and $BaLiI_3$ perovskites in the (100) plane is plotted and shown in Fig. 4(b, d, f, and h), respectively. It is evident from the figures that the electron distribution around the Ba^{2+} and X^- ions (X = F, Cl, Br, or I) are almost perfectly spherical. This finding indicates that the Ba-X bonds within the cubic $BaLiF_3$, $BaLiCl_3$, $BaLiBr_3$, and $BaLiI_3$ perovskites are mostly ionic. Hence, the materials can be categorized as ionic crystals.

Elastic Properties

The elastic properties of the compounds are summarized in Table 3, while the equations used in calculating the elastic properties are presented in our previous study [82].

The mechanical stability of materials is a significant property for applying materials in devices. In general, the mechanical stability of a compound is evaluated using the Born-Huang mechanical stability criteria [83]. Materials are mechanically stable if their elastic constants satisfy $C_{11} > 0$, $C_{44} > 0$, $(C_{11}-C_{12}) > 0$, $(C_{11} + 2C_{12}) > 0$, and $C_{12} < B < C_{11}$. Evaluation of the elastic

Table 3. Elastic properties of the cubic $BaLiX_3$ (X = F, Cl, Br, or I) perovskites calculated using the GGA functional

Parameters	Compounds			
	$BaLiF_3$	$BaLiCl_3$	$BaLiBr_3$	$BaLiI_3$
Elastic Const. C_{11} (GPa)	118.88	61.02	49.30	37.05
Elastic Const. C_{12} (GPa)	42.76	19.68	16.11	12.56
Elastic Const. C_{44} (GPa)	43.19	18.66	14.31	10.34
Bulk modulus B (GPa)	68.14	33.46	27.17	20.72
Shear modulus G (GPa)	41.06	19.44	15.19	11.06
Pugh Ratio B/G	1.66	1.72	1.79	1.87
Anisotropy Factor A	1.14	0.90	0.86	0.84
Young modulus E (GPa)	102.57	48.85	38.41	28.17
Poisson Ratio ϑ	0.25	0.26	0.27	0.27
Kleinman Parameter ζ	0.50	0.47	0.47	0.48
Cauchy Pressure $(C_{11}-C_{12})$	76.12	41.34	33.19	24.49
Debye Temperature θ_D (K)	398.25	270.62	199.37	151.88
Melting Temperature T_m (K)	1255.7 ± 300	913.69 ± 300	844.41 ± 300	772.0 ± 300
Average sound velocity V_m (m/s)	3164.09	2606.31	2040.65	1690.43
Longitudinal Sound Velocity V_l (m/s)	3673.34	3078.78	2455.68	2079.83
Transverse Sound Velocity V_t (m/s)	2851.51	2346.50	1835.98	1519.42
Lame Const. λ	41.03	21.00	17.75	13.02
Lame Const. μ	41.03	19.38	15.12	11.09

constants and the bulk moduli in Table 3 based on this criterion shows that all studied perovskites in the present work are mechanically stable. In addition, C_{11} of the four compounds is considerably larger than C_{12} and C_{14}. This large value of C_{11} is due to the directional Li-X ionic bond within the $BaLiX_3$ (X = F, Cl, Br, or I) compounds, as discussed in the previous section.

Another important property related to the elastic constants is the bulk modulus (B), representing the resistance of a material to applied external pressure. It is apparent from Table 3 that the elastic constants and the bulk modulus of $BaLiF_3$ are significantly larger than those of $BaLiCl_3$, $BaLiBr_3$, and $BaLiI_3$. This finding implies that $BaLiF_3$ has the most substantial resistance of all. Similarly, $BaLiF_3$ is predicted to have the largest shear modulus (41.06 GPa), substantially more significant than the shear modulus of $BaLiCl_3$ (19.44 GPa), $BaLiBr_3$ (15.19 GPa), and $BaLiI_3$ (11.06 GPa). This fact demonstrates that $BaLiF_3$ has stronger shear resistance compared to the other three isoelectronic perovskites, although all of them still have relatively high shear resistance. In addition, since the Young modulus (E) represents the stiffness of materials, $BaLiF_3$ is expected to be significantly stiffer than the other three compounds due to its highest Young modulus. It is also found that for all studied perovskites, the Young modulus is larger than the bulk modulus, indicating that $BaLiX_3$ perovskites are more resistant to tension than the effect of compression.

Reddy et al. [84] have found a systematic relationship between the bulk modulus and the energy gap of some materials. The authors reported that the bulk modulus is linearly proportional to the band energy of the materials, which is consistent with the result in the present study. However, it should be noted that this relationship does not apply to all materials. For example, Li et al. [85] claimed that the trend is not generally true for alloys, as the band gap energy in alloy systems varies due to the combination of size and chemical effects [86].

The Poisson ratio and Pugh's ratio can be used to evaluate the ductility or brittleness of materials. A material is ductile if its Poisson ratio is larger than 0.26 and brittle if it is lower than 0.26 [41]. From Table 3, the Poisson ratio of $BaLiF_3$ is 0.25, strongly indicating its brittle behavior. This is in excellent accordance with the previous studies [16-17]. The ductility and brittleness of the compound can be further verified by its Pugh's ratio [87]: materials are ductile if their Pugh's ratio is larger than 1.75. As its Pugh's ratio is 1.66 (Table 3), it is anticipated that $BaLiF_3$ is brittle.

Interestingly, the Poisson ratio and the Pugh ratio of the perovskites are found to increase following the replacement of F by Cl, Br, or I, which implies a decrease in their brittleness. With the Poisson and Pugh ratios of 0.26 and 1.72, respectively, $BaLiCl_3$ still possesses brittle behavior despite being less brittle than $BaLiF_3$. More importantly, it was found that $BaLiBr_3$ and $BaLiI_3$ are malleable. The change of behavior from brittle to ductile by changing halogens is an essential finding since ductile materials can be quickly deposited as high-quality thin films for various applications [3,88]. This phenomenon is also an alternative way to change the brittle behavior of compounds in addition to increasing applied pressure [17].

Furthermore, the Poisson ratio can be used to study the bonding character within solids. A value of Poisson ratio close to 0.25 implies that the material is an ionic crystal due to the central force within the material [17,89]. The computed Poisson ratio values for all perovskites in this study range between 0.25 and 0.27, indicating that these materials are ionic crystals, consistent with our previous discussions regarding the electronic density plots.

The first Lamé's constant λ measures the compressibility of materials, while the second constant μ is related to the shear stiffness of materials [90-91]. As seen from Table 3, the two constants λ and μ of $BaLiF_3$ are significantly larger than those of $BaLiCl_3$, $BaLiBr_3$, and $BaLiI_3$. This fact has been anticipated since it is well-known that the two constants are directly proportional to the Young modulus. Also, the values of the second constant μ resemble those of the shear modulus, which was true for many other isoelectronic compounds presented in Refs [92-95].

The Kleinman parameter ζ represents the internal strain of materials [90]. The value of ζ is between 0 and 1 for solids. $\zeta = 0$ corresponds to minimizing bond

bending, while $\zeta = 1$ is related to minimizing bond stretching [96]. The computed Kleinman parameter ζ for $BaLiF_3$, $BaLiCl_3$, $BaLiBr_3$, and $BaLiI_3$ are 0.50, 0.47, 0.47, and 0.48 for the respective perovskites. This fact suggests that the bond bending and the bond stretching are equal for $BaLiF_3$, while the bond bending within $BaLiCl_3$, $BaLiBr_3$, and $BaLiI_3$ compounds are slightly more dominant than the bond stretching.

Table 3 also shows that $BaLiF_3$ has the highest Debye temperature θ_D (398.25 K), significantly higher than $BaLiCl_3$ (270.62 K), $BaLiBr_3$ (199.37), and $BaLiI_3$ (151.88 K). This finding follows that the Debye temperature of materials is closely related to their specific heat, melting temperature, and elastic constants [91].

Some elastic properties of $BaLiF_3$ have been investigated both experimentally and theoretically. Therefore, a comparison with these previous values is necessary. Table 4 depicts the elastic properties of $BaLiF_3$ along with previously reported values. Overall, the three elastic constants, the bulk modulus, and the shear modulus of $BaLiF_3$ calculated using GGA functional in the present study and other GGA-based theoretical results in Table 4 are closer to the corresponding experimental values compared with Local Density Approximation (LDA)-based theoretical calculation. This does not necessarily mean that the GGA function is always more accurate than the LDA function in the study of the elastic properties of materials, as Råsander and Moram [97] showed that the performance of functionals is system-dependent. The authors evaluated the performance of various functionals in predicting the elastic properties of some insulators and semiconductors and found that the LDA is more accurate for some particular compounds.

It is important to note that some elastic properties of $BaLiF_3$ do not currently have experimental values. Therefore, our theoretical results and those in the literature are of great importance for further studies on this perovskite. Also, as previously mentioned, the elastic properties for $BaLiCl_3$, $BaLiBr_3$, and $BaLiI_3$ are presented for the first time in this work. The excellent agreement between the current theoretical results for $BaLiF_3$ and its corresponding experimental values and other theoretical results strongly indicates that our results for $BaLiCl_3$, $BaLiBr_3$, and $BaLiI_3$ can be considered a reliable prediction of the materials' properties.

Table 4. Comparison of elastic properties of the cubic $BaLiF_3$ from the present study using the GGA with other theoretical calculations and experiments

Parameters	This work	Other theoretical results	Experiment
Elastic Const. C_{11} (GPa)	118.88	GGA: 149.2 [39], 134.0 [17] LDA: 232.3 [39], 163.84 [10]	130 ± 1 [11]
Elastic Const. C_{12} (GPa)	42.76	GGA: 33.1 [39], 45.4 [17] LDA: 31.2 [39], 50.81 [10]	46.5 ± 0.5 [11]
Elastic Const. C_{44} (GPa)	43.19	GGA: 58.0 [39], 46.5 [17] LDA: 42.2 [39], 60.02 [10]	48.7 ± 0.5 [11]
Bulk modulus B (GPa)	68.14	GGA: 74.9 [17], 64.45 [10], 66.46 [14] LDA: 88.84 [10]	79 [11]
Shear modulus G (GPa)	41.06	GGA: 58.0 [39], 45.6 [17] LDA: 65.5 [39]	45.9 [11]
Poisson Ratio ϑ	0.25	GGA: 0.25 [17]	-
Pugh Ratio B/G	1.66	GGA: 1.64 [17]	-
Anisotropy Factor A	1.14	GGA: 1.12 [16]	-
Transverse Sound Velocity V_t (m/s)	2851.51	GGA: 2822.93 [16]	-
Longitudinal Sound Velocity V_l (m/s)	3673.34	GGA: 4873.80 [16]	-
Average sound velocity V_m (m/s)	3164.09	GGA: 3133.10 [16]	-
Debye Temperature θ_D (K)	398.25	GGA: 290.72 [16]	-

Table 4 indicates that there is a discrepancy between the C_{11} value (118.88 GPa) obtained in this study compared to that reported in references [17] (134.0 GPa) and [39] (149.2 GPa). The reason for this discrepancy is the use of different methods in the calculation despite using the GGA functional. In the present study, we used the thermo_pw code under Quantum Espresso. At the same time, Ref [17] implemented the CASTEP code, and Ref [39] used the all-electron linear muffin-tin orbital method in the full-potential implementation. Different packages imply different computational approaches, and therefore different results are expected. However, the accuracy of the methods can be evaluated in this case since the experimental value of C_{11} of $BaLiF_3$ is known, i.e., 130 GPa [11]. The % errors of C_{11} from the CASTEP code (3.07%) are smaller than those from our results using the thermo_pw package (8.55%) and the linear muffin-tin orbital method used in [39] (14.77%). This trend is also observed when evaluating the accuracy of the three methods in obtaining some other elastic properties, including C_{12}, C_{44}, and the shear modulus (G). These findings strongly suggest the CASTEP code used in [17] is expected to be more accurate than the thermo_pw code, which is also more accurate than the all-electron linear muffin-tin orbital method used in Ref [39] when calculating elastic properties.

Optical Properties

Optical properties of the $BaLiX_3$ (X = F, Cl, Br, or I) perovskites were successfully calculated, and the results within the photon energy interval 0–20 eV are presented and discussed in this section.

The imaginary part of the dielectric function $\varepsilon_2(\omega)$ and the real part of the dielectric function $\varepsilon_2(\omega)$ can be calculated using Eq. (4) and Eq. (5), respectively [98-100].

$$\varepsilon_2(\omega) = \frac{2e^2\pi}{\Omega\varepsilon_0} \sum_{K,V,C} \left| \left\langle \Psi_k^C \left| \hat{U}.\vec{r} \right| \Psi_k^V \right\rangle \right|^2 \delta\left(E_K^C - E_K^V - E\right) \quad (4)$$

$$\varepsilon_1(\omega) = 1 + \frac{2}{\pi} P \int_0^\infty \frac{\omega' \varepsilon_2(\omega')}{\omega'^2 - \omega^2} d\omega' \quad (5)$$

where e and Ω are the electronic charges and the unit cell volume, respectively; ψ_k^V and ψ_k^C are wave functions at a particular k in the valence band and the conduction band, respectively; E_K^C and E_K^V represent the energy of electrons at a special k in the conduction and the valence bands, respectively; Û is the unit vector in the direction of the polarization of the incident electric field of the light; δ is the delta function to account for the energy and momentum conservation during a transition.

After $\varepsilon_2(\omega)$ and $\varepsilon_1(\omega)$ are obtained, the refractive index as a function of photon energy $\eta(\omega)$ and the extinction coefficient $k(\omega)$ of the perovskites are calculated using Eq. (6) and (7), respectively [99].

$$\eta(\omega) = \frac{1}{\sqrt{2}} \left[\left(\varepsilon_1(\omega)^2 + \varepsilon_2(\omega)^2 \right)^{1/2} + \varepsilon_1(\omega) \right]^{1/2} \quad (6)$$

$$k(\omega) = \frac{1}{\sqrt{2}} \left[\left(\varepsilon_1(\omega)^2 + \varepsilon_2(\omega)^2 \right)^{1/2} - \varepsilon_1(\omega) \right]^{1/2} \quad (7)$$

The computed values of the real part of the dielectric function $\varepsilon_1(\omega)$, the imaginary part of the dielectric function $\varepsilon_2(\omega)$, the refractive index $\eta(\omega)$, and the extinction coefficient $k(\omega)$ of the $BaLiX_3$ (X = F, Cl, Br, or I) perovskites compounds within 0–20 eV are plotted in Fig. 5.

Fig. 5(a) shows the appearance of the highest peak of $\varepsilon_1(\omega)$ for $BaLiF_3$ (5.04) at 8.58 eV, which corresponds well with previous studies where the highest peak was observed at 8.6 eV [14-15]. Although the numerical value of the prominent peak was not explicitly stated in [10,16], it can be seen from their curve that the central peak was located at about 9 eV. Meanwhile, the static dielectric function $\varepsilon_1(0)$ of $BaLiF_3$ is found to be 2.57 in this study, which is also consistent with the previous reports, i.e., 2.5 [14], 2.6 [15], and about 1.96 [10,16]. In addition, the main feature of $\varepsilon_1(\omega)$ for $BaLiF_3$ obtained in this study is in excellent agreement with previous studies.

Fig. 5(a) also presents the real part of the dielectric function $\varepsilon_1(\omega)$ of $BaLiCl_3$, $BaLiBr_3$, and $BaLiI_3$, where a clear shift of the main peak to lower photon energy and an increase in static dielectric function are observed. The main peaks for the respective perovskites are observed at 5.72, 4.84, and 3.74 eV, whereas the static dielectric function values $\varepsilon_1(0)$ were found at 3.35, 3.83, and 4.56. It is important to note that the real part of the dielectric function $\varepsilon_1(\omega)$ is shifted toward lower photon energies as we move from F to Cl, Br, or I, which is also true for

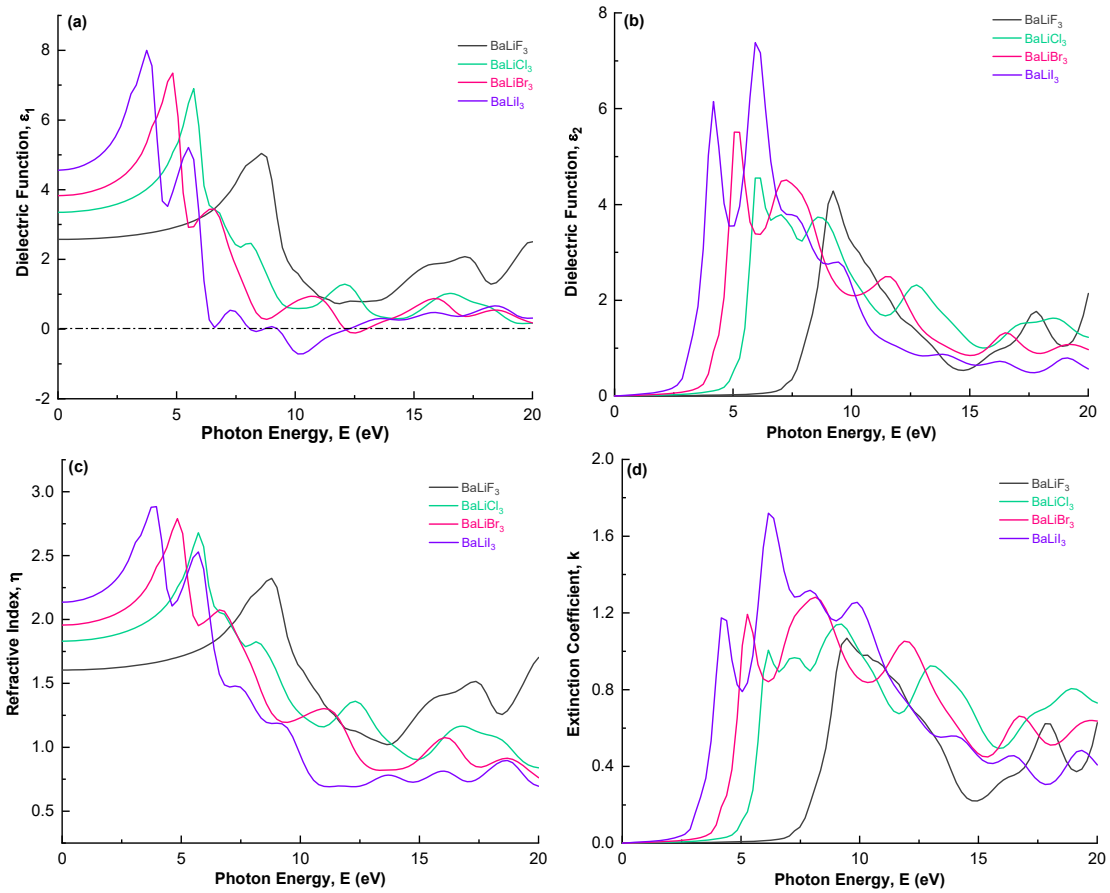

Fig 5. $\varepsilon_1(\omega)$ (a), $\varepsilon_2(\omega)$ (b), $\eta(\omega)$ (c), and $k(\omega)$ (d) of the cubic $BaLiX_3$ (X = F, Cl, Br, or I)

other optical properties presented in Fig. 5(b-d), Fig. 6(a-c). This trend is in close agreement with the electronic band structure of the compounds, as previously discussed, where the electronic band gaps of the materials decrease when Cl, Br, or I replace F. Additionally, the static dielectric function values $\varepsilon_1(0)$ are inversely proportional to the band gap energy of the compounds, which is also consistent with the Penn model [101]. Moreover, since a material with a larger static dielectric constant generally has better optoelectronic properties due to a lower rate of charge recombination [100,102-103], $BaLiI_3$ is predicted to possess better optoelectronic properties compared to $BaLiBr_3$, $BaLiCl_3$, and $BaLiF_3$ perovskites. A similar trend was also reported recently [104], where $FrGeF_3$ which has a larger static dielectric constant than $KGeF_3$ and $RbGeF_3$, was found to demonstrate better optoelectronic performance than $KGeF_3$ and $RbGeF_3$.

Fig. 5(b) presents the imaginary part of the dielectric function $\varepsilon_2(\omega)$, which represents the absorption behavior of the perovskites and, therefore, should be directly related to the band structure. It is evident from Fig. 5(b) that the threshold energy for the dielectric function $\varepsilon_2(\omega)$, i.e., the energy at which materials start absorbing light, shifts towards lower energy as F is replaced by Cl, Br, or I. This finding is consistent with the band structure and DOS of the materials, as depicted in Fig. 3, where the forbidden gap between valence and conduction bands of the compounds decreases due to the halogen replacement. The prominent absorption peaks for the $BaLiF_3$, $BaLiCl_3$, $BaLiBr_3$, and $BaLiI_3$ are at 9.24, 5.94, 5.06, and 5.94 eV, respectively. More importantly, Fig. 5(b) strongly reveals that $BaLiCl_3$, $BaLiBr_3$, and $BaLiI_3$ perovskites have a much more comprehensive absorption range compared to $BaLiF_3$ and that $BaLiI_3$ has the widest absorption range within 0–20 eV, followed by $BaLiBr_3$, $BaLiCl_3$, and $BaLiF_3$. As before, the overall feature of the $\varepsilon_2(\omega)$ curve in this study agrees very well with previous studies [10,14-16].

As expected, the refractive index of $BaLiX_3$ as a function of energy η(ω) (Fig. 5(c)) is very similar in shape to $\varepsilon_1(\omega)$ (Fig. 5(a)). The computed static refractive index η(0) of $BaLiF_3$ is 1.60, which is in excellent agreement with the corresponding predicted value of 1.59 by [14-15], and is slightly larger than a value of 1.40 reported by Yalcin et al. [16] and Korba et al. [10]. Meanwhile, the computed static refractive index η(0) for $BaLiCl_3$, $BaLiBr_3$, and $BaLiI_3$ are 1.83, 1.96, and 2.14, respectively. Additionally, the most significant values of the refractive index of $BaLiX_3$ (X = F, Cl, Br, or I) are 2.32 (at 8.80 eV), 2.68 (at 5.72 eV), 2.79 (at 4.84 eV), and 2.88 (at 3.96 eV), respectively.

As for the extinction coefficient k(ω) (Fig. 5(d)), it is well known that the feature of extinction coefficient k(ω) should resemble that of $\varepsilon_2(\omega)$, which is also the case in the present study. In addition, Eq. (6) clearly indicates that a local maximum of k(ω) should correspond to a local minimum of $\varepsilon_1(\omega)$. The comparison of Fig. 5(a) and 5(d) confirms this. Finally, the most significant values of the k(ω) of $BaLiX_3$ (X = F, Cl, Br, and I) within 0–20 eV are 1.07 (at 9.46 eV), 1.14 (at 9.24 eV), 1.28 (at 8.14 eV), and 1.69 (at 6.38 eV), respectively.

The reflectivity R(ω), the absorption coefficient α(ω), and the loss function L(ω) of the $BaLiX_3$ compounds are also essential properties that can be used to evaluate the potential of the materials for applications in devices. R(ω), L(ω), and α(ω) were calculated using Eq. (8-10) [99]. Fig. 6 depicts computed values of R(ω), α(ω) and L(ω) of the perovskites.

$$R(\omega)=\frac{(\eta-1)^2+k^2}{(\eta+1)^2+k^2} \tag{8}$$

$$\alpha(\omega)=\frac{2\omega}{c}k(\omega) \tag{9}$$

$$L(\omega)=\frac{\varepsilon^2}{\varepsilon_1^{\,2}+\varepsilon_2^{\,2}} \tag{10}$$

Fig. 6(a) shows that all studied compounds have low reflectivity, which is suitable for device applications.

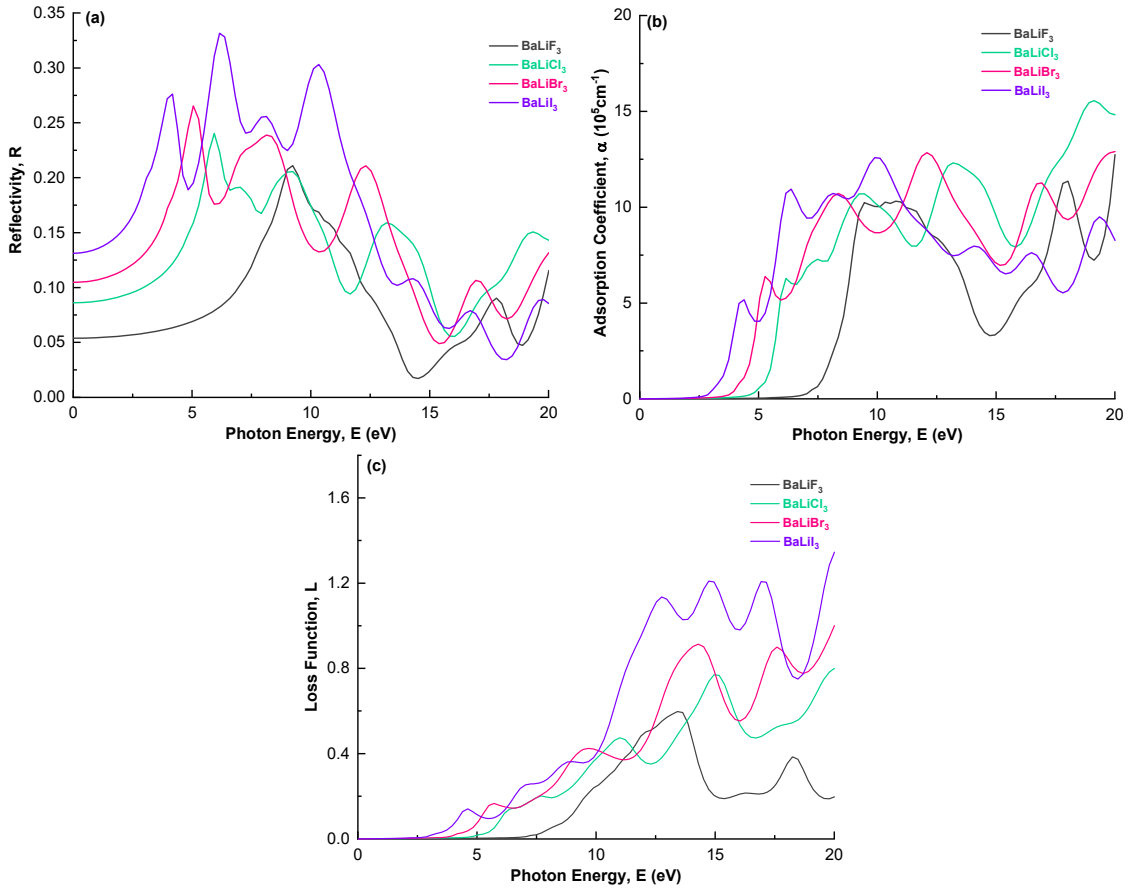

Fig 6. R(ω) (a), α(ω) (b), and L(ω) (c) of cubic $BaLiX_3$ (X = F, Cl, Br, and I)

Overall, $BaLiI_3$ has the highest reflectivity, respectively followed by $BaLiBr_3$, $BaLiCl_3$, and $BaLiF_3$ within 0–15 eV. Between 15 and 20 eV, $BaLiCl_3$ is predicted to have slightly higher reflectivity than the others. The highest reflectivity of $BaLiI_3$ is about 33.14% (at 6.16 eV), followed by $BaLiBr_3$: 26.53% (at 5.06 eV), $BaLiCl_3$: 24.02% (at 5.94 eV), and $BaLiF_3$: 21.10% (at 9.24 eV). The general feature of reflectivity in this study matches very well with that reported by Mousa et al. [15] and Mubarak and Mousa [14].

The considerable absorption of $BaLiF_3$ was previously predicted by Mousa et al. [15]. This prediction is confirmed here, where the absorption coefficient $\alpha(\omega)$ of $BaLiF_3$ is in the order of 10^5 cm^{-1} (Fig. 6(b)). Similar absorption behavior is also predicted for $BaLiCl_3$, $BaLiBr_3$, and $BaLiI_3$. Another important finding from Fig. 6(b) is that $BaLiCl_3$, $BaLiBr_3$, and $BaLiI_3$ perovskites have a much broader absorption range compared to $BaLiF_3$, implying that they can be applied in a wider range of applications.

As $L(\omega)$ represents an inelastic scattering process, Fig. 6(c) shows that inelastic scattering is negligible for low photon energy. A comparison of Fig. 6(c) and 6(b) suggests that the threshold values of the absorption coefficients and the loss function are in good agreement, as expected. This finding implies that the scattering process becomes more apparent when the materials absorb incident light. Above the threshold values, the loss function of the $BaLiCl_3$, $BaLiBr_3$, and $BaLiI_3$ materials increases up to 20 eV while that of $BaLiF_3$ increases to peak at about 13 eV and then decreases. Overall, across the whole energy range 0–20 eV, the highest loss function is experienced by $BaLiI_3$, followed by $BaLiBr_3$, $BaLiCl_3$, and $BaLiF_3$ compounds.

■ CONCLUSION

Theoretical DFT predictions of the structural, electronic, elastic and optical properties of the $BaLiX_3$ (X = F, Cl, Br, or I) perovskites are reported for the first time in the present study. The properties of $BaLiF_3$ agreed very well with experimental and other theoretical results in the literature. The optimized lattice constants of the $BaLiX_3$ (X = F, Cl, Br, or I) compounds increased when Cl, Br replace F or I, while the reverse was true for their electronic band gaps. The exceptional optical properties of these materials and their mechanical stability suggest that they are suitable for various applications.

■ ACKNOWLEDGMENTS

This research is supported by a 2023 DIPA grant provided by the Faculty of Science and Engineering, the University of Nusa Cendana, with contract's number: 10/UN15.15.3.PPK/SPP/FST/IV/2023.

■ AUTHOR CONTRIBUTIONS

Redi Kristian Pingak wrote the original draft of the manuscript; Redi Kristian Pingak, Soukaina Bouhmaidi, and Larbi Setti conducted the DFT calculations; Redi Kristian Pingak, Soukaina Bouhmaidi, Larbi Setti, Bartholomeus Pasangka, Bernandus, Hadi Imam Sutaji, Fidelis Nitti, and Meksianis Zadrak Ndii wrote and revised the manuscript as well as interpreting the results. All authors agreed to the final version of this manuscript.

■ REFERENCES

[1] Zhang, L., Zhuang, Z., Fang, Q., and Wang, X., 2022, Study on the automatic identification of ABX_3 perovskite crystal structure based on the bond-valence vector sum, *Materials*, 16 (1), 334.

[2] Wang, Y., Tang, Y., Jiang, J., Zhang, Q., Sun, J., Hu, Y., Cui, Q., Teng, F., Lou, Z., and Hou, Y., 2020, Mixed-dimensional self-assembly organic–inorganic perovskite microcrystals for stable and efficient photodetectors, *J. Mater. Chem. C*, 8 (16), 5399–5408.

[3] Roknuzzaman, M., Alarco, J.A., Wang, H., Du, A., Tesfamichael, T., and Ostrikov, K., 2019, *Ab initio* atomistic insights into lead-free formamidinium based hybrid perovskites for photovoltaics and optoelectronics, *Comput. Mater. Sci.*, 169, 109118.

[4] Roknuzzaman, M., Ostrikov, K., Wang, H., Du, A., and Tesfamichael, T., 2017, Towards lead-free perovskite photovoltaics and optoelectronics by *ab-initio* simulations, *Sci. Rep.*, 7, 14025.

[5] Tao, Q., Xu, P., Li, M., and Lu, W., 2021, Machine learning for perovskite materials design and discovery, *npj Comput Mater.*, 7, 23.

[6] Veldhuis, S.A., Boix, P.P., Yantara, N., Li, M., Sum,

T.C., Mathews, N., and Mhaisalkar, S.G., 2016, Perovskite materials for light-emitting diodes and lasers, *Adv. Mater.*, 28 (32), 6804–6834.

[7] Li, L., Tian, G., Chang, W., Yan, Y., Ling, F., Jiang, S., Xiang, G., and Zhou, X., 2020, A novel double-perovskite $LiLaMgTeO_6:Mn^{4+}$ far-red phosphor for indoor plant cultivation white LEDs: Crystal and electronic structure, and photoluminescence properties, *J. Alloys Compd.*, 832, 154905.

[8] Ekström, E., le Febvrier, A., Bourgeois, F., Lundqvist, B., Palisaitis, J., Persson, P.O.A., Caballero-Calero, O., Martín-González, M.S., Klarbring, J., Simak, S.I., Eriksson, F., Paul, B., and Eklund, P., 2020, The effects of microstructure, Nb content and secondary Ruddlesden–Popper phase on thermoelectric properties in perovskite $CaMn_{1-x}Nb_xO_3$ (x = 0-0.10) thin films, *RSC Adv.*, 10 (13), 7918–7926.

[9] Sydorchuk, V. Lutsyuk, I., Shved, V., Hreb, V., Kondyr, A., Zakutevskyy, O., and Vasylechko, L., 2020, $PrCo_{1-x}Fe_xO_3$ perovskite powders for possible photocatalytic applications, *Res. Chem. Intermed.*, 46 (3), 1909–1930.

[10] Korba, S.A., Meradji, H., Ghemid, S., and Bouhafs, B., 2009, First principles calculations of structural, electronic and optical properties of $BaLiF_3$, *Comput. Mater. Sci.*, 44 (4), 1265–1271.

[11] Boumriche, A., Gesland, J.Y., Bulou, A., Rousseau, M., Fourquet, J.L., and Hennion, B., 1994, Structure and dynamics of the inverted perovskite $BaLiF_3$, *Solid State Commun.*, 91 (2), 125–128.

[12] Düvel, A., Wilkening, M., Uecker, R., Wegner, S., Šepelák, V., and Heitjans, P., 2010, Mechanosynthesized nanocrystalline $BaLiF_3$: The impact of grain boundaries and structural disorder on ionic transport, *Phys. Chem. Chem. Phys.*, 12 (37), 11251–11262.

[13] Mishra, A.K., Garg, N., Shanavas, K.V., Achary, S.N., Tyagi, A.K., and Sharma, S.M., 2011, High pressure structural stability of $BaLiF_3$, *J. Appl. Phys.*, 110 (12), 123505.

[14] Mubarak, A.A., and Mousa, A.A., 2012, The electronic and optical properties of the fluoroperovskite $BaXF_3$ (X = Li, Na, K, and Rb) compounds, *Comput. Mater. Sci.*, 59, 6–13.

[15] Mousa, A.A., Mahmoud, N.T., and Khalifeh, J.M., 2013, The electronic and optical properties of the fluoroperovskite $XLiF_3$ (X = Ca, Sr, and Ba) compounds, *Comput. Mater. Sci.*, 79, 201–205.

[16] Yalcin, B.G., Salmankurt, B., and Duman, S., 2016, Investigation of structural, mechanical, electronic, optical, and dynamical properties of cubic $BaLiF_3$, $BaLiH_3$ and $SrLiH_3$, *Mater. Res. Express*, 3, 036301.

[17] Lv, Z.L., Cui, H.L., Wang, H., Li, X.H., and Ji, G.F., 2016, Electronic and elastic properties of $BaLiF_3$ with pressure effects: First principles study, *Phys. Status Solidi B*, 253 (9), 1788–1794.

[18] Chowdhury, N., Riesen, N., and Riesen, H., 2019, Efficient generation of stable Sm^{2+} in nanocrystalline $BaLiF_3:Sm^{3+}$ by UV- and X-irradiation, *J. Phys. Chem. C*, 123 (41), 25477–25481.

[19] Song, X., Zhao, Y., Wang, X., Ni, J., Meng, S., and Dai, Z., 2023, Strong anharmonicity and high thermoelectric performance of cubic thallium-based fluoride perovskites $TlXF_3$ (X = Hg, Sn, Pb), *Phys. Chem. Chem. Phys.*, 25 (7), 5776–5784.

[20] Huang, Y.T., Kavanagh, S.R., Scanlon, D.O., Walsh, A., and Hoye, R.L.Z., 2021, Perovskite-inspired materials for photovoltaics and beyond-from design to devices, *Nanotechnology*, 32 (13), 132004.

[21] Pingak, R.K., 2022, A DFT study of structural and electronic properties of cubic thallium based fluoroperovskites $TlBF_3$ (B = Ge, Sn, Pb, Zn, Cd, Hg, Mg, Ca, Sr, Ba), *Comput. Condens. Matter*, 33, e00747.

[22] Lynn, M.O., Ologunagba, D., Dangi, B.B., and Kattel, S., 2023, Density functional theory study of bulk properties of transition metal nitrides, *Phys. Chem. Chem. Phys.*, 25 (6), 5156–5163.

[23] Sholihun, S., Kadarisman, H.P., and Nurwantoro, P., 2018, Density-functional-theory calculations of formation energy of the nitrogen-doped diamond, *Indones. J. Chem.*, 18 (4), 749–754.

[24] Hutama, A.S., Marlina, L.A., Chou, C.P., Irle, S., and Hofer, T.S., 2021, Development of density-functional tight-binding parameters for the molecular dynamics simulation of zirconia, yttria,

and yttria-stabilized zirconia, *ACS Omega*, 6 (31), 20530–20548.

[25] Hauwali, N.U.J., Syuhada, I., Rosikhin, A., and Winata, T., 2021, Fundamental properties of parallelogram graphene nanoflakes: A first principle study, *Mater. Today: Proc.*, 44, 3305–3308.

[26] Prasetyo, N., and Pambudi, F.I., 2021, Toward hydrogen storage material in fluorinated zirconium metal-organic framework (MOF-801): A periodic density functional theory (DFT) study of fluorination and adsorption, *Int. J. Hydrogen Energy*, 46 (5), 4222–4228.

[27] Hutama, A.S., Huang, H., and Kurniawan, Y.S., 2019, Investigation of the chemical and optical properties of halogen-substituted *N*-methyl-4-piperidone curcumin analogs by density functional theory calculations, *Spectrochim. Acta, Part A*, 221, 117152.

[28] Pradipta, M.F., Pranowo, H.D., Alfiyah, V., and Hutama, A.S., 2021, Theoretical study of oxygen atom adsorption on a polycyclic aromatic hydrocarbon using density-functional theory, *Indones. J. Chem.*, 21 (5), 1072–1085.

[29] Hutama, A.S., Hijikata, Y., and Irle, S., 2017, Coupled cluster and density functional studies of atomic fluorine chemisorption on coronene as model systems for graphene fluorination, *J. Phys. Chem. C*, 121 (27), 14888–14898.

[30] Amalia, W., Nurwantoro, P., and Sholihun, S., 2018, Density-functional-theory calculations of structural and electronic properties of vacancies in monolayer hexagonal boron nitride (h-BN), *Comput. Condens. Matter*, 18, e00354.

[31] Giannozzi, P., Baroni, S., Bonini, N., Calandra, M., Car, R., Cavazzoni, C., Ceresoli, D., Chiarotti, G.L., Cococcioni, M., Dabo, I., Dal Corso, A., Stefano, de Gironcoli, S., Fabris, S., Fratesi, G., Gebauer, R., Gerstmann, U., Gougoussis, C., Kokalj, A., Lazzeri, M., Martin-Samos, L., Marzari, N., Mauri, F., Mazzarello, R., Paolini, S., Pasquarello, A., Paulatto, L., Sbraccia, C., Scandolo, S., Sclauzero, G., Seitsonen, A.P., Smogunov, A., Umari, P., and Wentzcovitch, R.M., 2009, QUANTUM ESPRESSO: A modular and open-source software project for quantum simulations of materials, *J. Phys.: Condens. Matter*, 21 (39), 395502.

[32] Perdew, J.P., Burke, K., and Ernzerhof, M., 1996, Generalized gradient approximation made simple, *Phys. Rev. Lett.*, 77 (18), 3865–3868.

[33] Pitriana, P., Wungu, T.D.K., Herman, H., and Hidayat, R., 2019, The characteristics of band structures and crystal binding in all-inorganic perovskite $APbBr_3$ studied by the principle calculations using the density functional theory (DFT) method, *Results Phys.*, 15, 102592.

[34] Behzadi, P., Ketabi, S.A., and Amiri, P., 2021, First-principles investigation of the electronic and optical properties of As_2GeTe nanotubes, *Solid State Commun.*, 336, 114421.

[35] Johannes, A.Z., 2018, Simulasi perubahan densitas muatan adsorpsi atom hydrogen-grafena dengan teori fungsi kerapatan, *JFiSA*, 3 (2), 179–184.

[36] Birch, F., 1947, Finite elastic strain of cubic crystals, *Phys. Rev.*, 71 (11), 809–824.

[37] Zhuravlev, K.K., 2007, PbSe vs. CdSe: Thermodynamic properties and pressure dependence of the band gap, *Phys. B*, 394 (1), 1–7.

[38] Hastuti, D.P., Nurwantoro, P., and Sholihun, S., 2019, Stability study of germanene vacancies: The first-principles calculations, *Mater. Today Commun.*, 19, 459–463.

[39] Vaitheeswaran, G., Kanchana, V., Zhang, X., Ma, Y., Svane, A., and Christensen, N.E., 2016, Calculated high-pressure structural properties, lattice dynamics and quasi particle band structures of perovskite fluorides $KZnF_3$, $CsCaF_3$ and $BaLiF_3$, *J. Phys.: Condens. Matter*, 28 (31), 315403.

[40] Sarukura, N., Murakami, H., Estacio, E., Ono, S., El Ouenzerfi, R., Cadatal, M., Nishimatsu, T., Terakubo, N., Mizuseki, H., Kawazoe, Y., Yoshikawa, A., and Fukuda, T., 2007, Proposed design principle of fluoride-based materials for deep ultraviolet light emitting devices, *Opt. Mater.*, 30 (1), 15–17.

[41] Ghaithan, H.M., Alahmed, Z.A., Qaid, S.M.H., and Aldwayyan, A.S., 2021, Density functional theory analysis of structural, electronic, and optical

properties of mixed-halide orthorhombic inorganic perovskites, *ACS Omega*, 6 (45), 30752–30761.

[42] Chen, K., Schünemann, S., Song, S., and Tüysüz, H., 2018, Structural effects on optoelectronic properties of halide perovskites, *Chem. Soc. Rev.*, 47 (18), 7045–7077.

[43] Ahmad, M., Rehman, G., Ali, L., Shafiq, M., Iqbal, R., Ahmad, R., Khan, T., Jalali-Asadabadi, S., Maqbool, M., and Ahmad, I., 2017, Structural, electronic and optical properties of $CsPbX_3$ (X = Cl, Br, I) for energy storage and hybrid solar cell applications, *J. Alloys Compd.*, 705, 828–839.

[44] Chen, Y., Feng, Z., Pal, A., and Zhang, J., 2022, Recent progress on the performance of lead-based halide perovskite $APbX_3$ detectors, *Phys. Status Solidi A*, 219 (9), 2200018.

[45] Thi Han, N., Khuong Dien, V., and Lin, M.F., 2022, Electronic and optical properties of $CsGeX_3$ (X = Cl, Br and I) compounds, *ACS Omega*, 7 (29), 25210–25218.

[46] Bouhmaidi, S., Marjaoui, A., Talbi, A., Zanouni, M., Nouneh, K., and Setti, L., 2022, A DFT study of electronic, optical and thermoelectric properties of Ge-halide perovskites $CsGeX_3$ (X = F, Cl and Br), *Comput. Condens. Matter*, 31, e00663.

[47] Hasan, N., Arifuzzaman, M., and Kabir, A., 2022, Structural, elastic, and optoelectronic properties of inorganic cubic $FrBX_3$ (B = Ge, Sn; X = Cl, Br, I) perovskite: The density functional theory approach, *RSC Adv.*, 12 (13), 7961–7972.

[48] Hamideddine, I., Tahiri, N., El Bounagui, O., and Ez-Zahraouy, H., 2022, Ab initio study of structural and optical properties of the halide perovskite KBX_3 compound, *J. Korean Ceram. Soc.*, 59, 350–358.

[49] Abdulkareem, N.A., Ilyas, B.M., and Sami, S.A., 2021, A first principle investigation of the non-synthesized cubic perovskite $LiGeX_3$ (X = I, Br, and Cl), *Mater. Sci. Semicond. Process.*, 131, 105858.

[50] Rahman, M.H., Jubair, M., Rahaman, M.Z., Ahasan, M.S., Ostrikov, K., and Roknuzzaman, M., 2022, $RbSnX_3$ (X = Cl, Br, I): Promising lead-free metal halide perovskites for photovoltaics and optoelectronics, *RSC Adv.*, 12 (12), 7497–7505.

[51] Ur Rehman, J., Usman, M., Amjid, S., Sagir, M., Bilal Tahir, M., Hussain, A., Alam, I., Nazir, R., Alrobei, H., Ullah, S., and Assiri, M.A., 2022, First-principles calculations to investigate structural, electronics, optical and elastic properties of Sn-based inorganic Halide-perovskites $CsSnX_3$ (X = I, Br, Cl) for solar cell applications, *Comput. Theor. Chem.*, 1209, 113624.

[52] Hayatullah, H., Murtaza, G., Muhammad, S., Naeem, S., Khalid, M.N., and Manzar, A., 2013, Physical properties of $CsSnM_3$ (M = Cl, Br, I): A first principle study, *Acta Phys. Pol. A*, 124 (1), 102–107.

[53] Rashid, M.A., Saiduzzaman, M., Biswas, A., and Hossain, K.M., 2022, First-principles calculations to explore the metallic behavior of semiconducting lead-free halide perovskites $RbSnX_3$ (X = Cl, Br) under pressure, *Eur. Phys. J. Plus*, 137, 649.

[54] Saiduzzaman, M., Ahmed, T., Hossain, K.M., Biswas, A., Mitro, S.K., Sultana, A., Alam, M.S., and Ahmad S., 2023, Band gap tuning of non-toxic Sr-based perovskites $CsSrX_3$ (X = Cl, Br) under pressure for improved optoelectronic applications, *Mater. Today Commun.*, 34, 105188.

[55] Harbi, A., and Moutaabbid, M., 2022, Thermoelectric and optoelectronic properties of novel lead-free halide perovskites $CsRbTiX_6$ (X= I, Br and Cl) for photovoltaic applications, *Comput. Condens. Matter*, 32, e00733.

[56] Zelai, T., Rouf, S.A., Mahmood, Q., Bouzgarrou, S., Amin, M.A., Aljameel, A.I., Ghrib, T., Hegazy, H.H., and Mera, A., 2022, First-principles study of lead-free double perovskites Ga_2PdX_6 (X = Cl, Br, and I) for solar cells and renewable energy, *J. Mater. Res. Technol.*, 16, 631–639.

[57] Sharma, R., Dey, A., Ahmed Dar, S., and Srivastava, V., 2021, A DFT investigation of $CsMgX_3$ (X = Cl, Br) halide perovskites: Electronic, thermoelectric and optical properties, *Comput. Theor. Chem.*, 1204, 113415.

[58] Mousa, A.A., Abu-Jafar, M.S., Dahliah, D., Shaltaf, R.M., and Khalifeh, J.M., 2018, Investigation of the perovskite $KSrX_3$ (X = Cl and F) compounds, examining the optical, elastic, electronic and

structural properties: FP-LAPW study, *J. Electron. Mater.*, 47 (1), 641–650.

[59] Mahmood, Q., Hedhili, F., Al-Shomar, S., Chebaaneef, S., Al-Muhimeed, T.I., AlObaid, A., Mera, A., and Alamri, O.A., 2021, Electronic, optical, and transport properties of $RbYbX_3$ (X = Cl, Br) for solar cells and renewable energy: A quantum DFT study, *Phys Scr.*, 96, 095806.

[60] Moreira, R.L., and Dias, A., 2007, Comment on "Prediction of lattice constant in cubic perovskites", *J. Phys. Chem. Solids*, 68 (8), 1617–1622.

[61] Trots, D.M., and Myagkota, S.V., 2008, High-temperature structural evolution of caesium and rubidium triiodoplumbates, *J. Phys. Chem. Solids*, 69 (10), 2520–2526.

[62] Tang, Y, Zhang, J., Zhong, X., Wang, Q., Zhang, H., Ren, C., and Wang, J., 2019, Revealing the structural, electronic and optical properties of lead-free perovskite derivatives of Rb_2SnX_6 (X = Cl, Br and I): A theory calculation, *Sol. Energy*, 190, 272–277.

[63] Aslam, F., Ullah, H., and Hassan, M., 2021, Theoretical investigation of Cs_2InBiX_6 (X = Cl, Br, I) double perovskite halides using first-principle calculations, *Mater. Sci. Eng., B*, 274, 115456.

[64] Saeed, M., Ul Haq, I., Ur Rehman, S., Ali, A., Shah, W.A., Ali, Z., Khan, Q., and Khan, I., 2021, Optoelectronic and elastic properties of metal halides double perovskites Cs_2InBiX_6 (X = F, Cl, Br, I), *Chin. Opt. Lett.*, 19 (3), 030004.

[65] Saeed, M., Ul Haq, I., Saleemi, A.S., Ur Rehman, S., Ul Haq, B., Chaudhry, A.R., and Khan, I., 2022, First-principles prediction of the ground-state crystal structure of double-perovskite halides Cs_2AgCrX_6 (X = Cl, Br, and I), *J. Phys. Chem. Solids*, 160, 110302.

[66] Iqbal, S., Mustafa, G.M., Asghar, M., Noor, N.A., Iqbal, M.W., Mahmood, A., and Shin, Y.H., 2022, Tuning the optoelectronic and thermoelectric characteristics of narrow bandgap Rb_2AlInX_6 (X = Cl, Br, I) double perovskites: A DFT study, *Mater. Sci. Semicond. Process.*, 143, 106551.

[67] Albalawi, H., Mustafa, G.M., Saba, S., Kattan, N.A., Mahmood, Q., Somaily, H.H., Morsi, M., Alharthi, S., and Amin, M.A., 2022, Study of optical and thermoelectric properties of double perovskites Cs_2KTlX_6 (X = Cl, Br, I) for solar cell and energy harvesting, *Mater. Today Commun.*, 32, 104083.

[68] Alotaibi, N.H., Mustafa, G.M., Kattan, N.A., Mahmood, Q., Albalawi, H., Morsi, M., Somaily, H.H., Hafez, M.A., Mahmoud, H.I., and Amin, M.A., 2022, DFT study of double perovskites Cs_2AgBiX_6 (X = Cl, Br): An alternative of hybrid perovskites, *J. Solid State Chem.*, 313, 123353.

[69] Niaz, S., Khan, M.A., Noor, N.A., Ullah, H., and Neffati, R., 2022, Bandgap tuning and thermoelectric characteristics of Sc-based double halide perovskites K_2ScAgZ_6 (Z = Cl, Br, I) for solar cells applications, *J. Phys. Chem. Solids*, 174, 111115.

[70] Johnson, A., Gbaorun, F., and Ikyo, B.A., 2022, First-principles study of $(CsMA)NaSbX_6$ (MA = methylammonium; X = Cl, Br, I) organic–inorganic hybrid double perovskites for optoelectronic applications, *J. Comput. Electron.*, 21 (1), 34–39.

[71] Khan, M.A., Alburaih, H.A., Noor, N.A., and Dahshan, A., 2021, Comprehensive investigation of opto-electronic and transport properties of Cs_2ScAgX_6 (X = Cl, Br, I) for solar cells and thermoelectric applications, *Sol. Energy*, 225, 122–128.

[72] Choudhary, S., Tomar, S., Kumar, D., Kumar, S., and Verma, A.S., 2021, Investigations of lead free halides in sodium based double perovskites Cs_2NaBiX_6 (X = Cl, Br, I): An *ab initio* study, *East Eur. J. Phys.*, 3, 74–80.

[73] Behera, D., and Mukherjee, S.K., 2022, Optoelectronics and transport phenomena in Rb_2InBiX_6 (X = Cl, Br) compounds for renewable energy applications: A DFT insight, *Chemistry*, 4 (3), 1044–1059.

[74] Kattan, N.A., Mahmood, Q., Nazir, G., Rehman, A., Sfina, N., Al-anazy, M.M., Sofi, S.A., Morsi, M., and Amin, M.A., 2023, Modifying electronic bandgap by halide ions substitution to investigate double perovskites Rb_2AgInX_6 (X = Cl, Br, I) for solar cells applications and thermoelectric characteristics, *Mater. Today Commun.*, 34, 105166.

[75] Ye, X., Liu, A., Zhao, Y., Han, Q., Kitamura, T., and Ma, T., 2022, DFT study of X-site ion substitution doping of Cs_2PtX_6 on its structural and electronic properties, *Int. J. Energy Res.*, 46 (6), 8471–8479.

[76] Al-Muhimeed, T.I., Alzahrani, J., Rouf, S.A., Al-Qaisi, S., Anbarasan, R., Mahmood, Q., Albalawi, H., Alharthi, S., Amin, M.A., and Somaily, H.H., 2022, Tuning of band gap by anion variation of Ga_2TiX_6 (X = Cl, Br, I) for solar cells and renewable energy, *Phys. Scr.*, 97 (8), 085815.

[77] Bhamu, K.C., Soni, A., and Sahariya, J., 2018, Revealing optoelectronic and transport properties of potential perovskites Cs_2PdX_6 (X = Cl, Br): A probe from density functional theory (DFT), *Sol. Energy*, 162, 336–343.

[78] Younas, M., Mahmood, Q., Kattan, N., Alshahrani, T., Mera, A., Mersal, G.A.M., Amin, M., and Somaily, H.H., 2022, Study of new double perovskites Tl_2PtX_6 (X = Cl, Br, I) for solar cells and thermoelectric applications, *Phys. Scr.,* 97 (12), 125803.

[79] Albalawi, H., Nazir, G., Younas, M., Al-Qaisi, S., Ashiq, M.G.B., Alzahrani, J., Somaily, H.H., Morsi, M., and Ghrib, T., 2022, Study of lead-free vacancy ordered double perovskites Cs_2TeX_6 (X = Cl, Br, I) for solar cells, and renewable energy, *Phys. Scr.,* 97, 095801.

[80] Mahmood, Q., Nazir, G., Bouzgarrou, S., Aljameel, A.I., Rehman, A., Albalawi, H., Ul Haq, B., Ghrib, T., and Mera, A., 2022, Study of new lead-free double perovskites halides Tl_2TiX_6 (X = Cl, Br, I) for solar cells and renewable energy devices, *J. Solid State Chem.,* 308, 122887.

[81] Callister, W.D., and Rethwisch, D.G., 2018, *Fundamentals of Materials Science and Engineering*, 5th Ed., John Wiley and Sons Inc., Hoboken, NJ, USA.

[82] Bouhmaidi, S., Azouaoui, A., Benzakour, N., Hourmatallah, A., and Setti, L., 2022, First principles calculations on structural, electronic, elastic, optical, and thermoelectric properties of thallium based chloroperovskites $TlMCl_3$ (M = Zn and Cd), *Comput. Condens. Matter*, 33, e00756.

[83] Born, M., 1940, On the stability of crystal lattices, *Math. Proc. Cambridge Philos. Soc.*, 36 (2), 160–172.

[84] Reddy, R.R., Gopal, K.R., Narasimhulu, K., Reddy, L.S.S., Kumar, K.R., Balakrishnaiah, G., and Kumar, M.R., 2009, Interrelationship between structural, optical, electronic and elastic properties of materials, *J. Alloys Compd.*, 473 (1-2), 28–35.

[85] Li, K., Kang, C., and Xue, D., 2012, Electronegativity calculation of bulk modulus and band gap of ternary ZnO-based alloys, *Mater. Res. Bull.*, 47 (10), 2902–2905.

[86] Song, Z., Fan, W., Tan, C.S., Wang, Q., Nam, D., Zhang, D.H., and Sun, G., 2019, Band structure of $Ge_{1-x}Sn_x$ alloy: A full-zone 30-band k·p model, *New J. Phys.*, 21 (7), 073037.

[87] Pugh, S.F., 1954, Relations between the elastic moduli and the plastic properties of polycrystalline pure metals, *Lond. Edinb. Dubl. Phil. Mag.*, 45 (367), 823–843.

[88] Krishnamoorthy, T., Ding, H., Yan, C., Leong, W.L., Baikie, T., Zhang, Z., Sherburne, M., Li, S., Asta, M., Mathews, N., and Mhaisalkar, S.G., 2015, Lead-free germanium iodide perovskite materials for photovoltaic applications, *J. Mater. Chem. A*, 3 (47), 23829–23832.

[89] Mattesini, M., Magnuson, M., Tasnádi, F., Höglund, C., Abrikosov, I.A., and Hultman, L., 2009, Elastic properties and electrostructural correlations in ternary scandium-based cubic inverse perovskites: A first-principles study, *Phys. Rev. B*, 79 (12), 125122.

[90] Shah, M.A.H., Nuruzzaman, M., Hossain, A., Jubair, M., and Zilani, M.A.K., 2023, A DFT insight into structural, mechanical, elasto-acoustic, and anisotropic properties of $AePdH_3$ (Ae = Ca, Sr, Ba) perovskites under pressure, *Comput. Condens. Matter*, 34, e00774.

[91] Ghebouli, B., Ghebouli, M.A., Bouhemadou, A., Fatmi, M., Khenata, R., Rached, D., Ouahrani, T., and Bin-Omran, S., 2012, Theoretical prediction of the structural, elastic, electronic, optical and thermal properties of the cubic perovskites $CsXF_3$ (X = Ca, Sr and Hg) under pressure effect, *Solid State Sci.*, 14 (7), 903–913.

[92] Bakar, A., Alrashdi, A.O., Fadhali, M.M., Afaq, A., Yakout H.A., and Asif, M., 2022, Effect of pressure

on structural, elastic and mechanical properties of cubic perovskites $XCoO_3$ (X = Nd, Pr) from first-principles investigations, *J. Mater. Res. Technol.*, 19, 4233–4241.

[93] Erum, N., and Iqbal, M.A., 2020, Elastomechanical and magneto-optoelectronic investigation of $RbCoF_3$: An *ab initio* DFT study, *Acta Phys. Pol., A*, 138 (3), 509–517.

[94] Mubarak, A.A., and Al-Omari, S., 2015, First-principles calculations of two cubic fluoroperovskite compounds: $RbFeF_3$ and $RbNiF_3$, *J. Magn. Magn. Mater.*, 382, 211–218.

[95] El Amine Monir, M., and Dahou, F.Z., 2020, Structural, thermal, elastic, electronic and magnetic properties of cubic lanthanide based perovskites type oxides PrXO3 (X = V, Cr, Mn, Fe): Insights from *ab initio* study, *SN Appl. Sci.*, 2 (3), 465.

[96] Cherif, Y.B., Rouaighia, M., Zaoui, A., and Boukortt, A., 2017, Optoelectronic, elastic and thermal properties of cubic perovskite-type $SrThO_3$, *Acta Phys. Pol., A*, 131 (3), 406–413.

[97] Råsander, M., and Moram, M.A., 2015, On the accuracy of commonly used density functional approximations in determining the elastic constants of insulators and semiconductors, *J. Chem. Phys.*, 143 (14), 144104.

[98] Green, M.A., Jiang, Y., Soufiani, A.M., and Ho-Baillie, A., 2015, Optical properties of photovoltaic organic-inorganic lead halide perovskites, *J. Phys. Chem. Lett.*, 6 (23), 4774–4785.

[99] Ambrosch-Draxl, C., and Sofo, J.O., 2006, Linear optical properties of solids within the full-potential linearized augmented plane wave method, *Comput. Phys. Commun.*, 175 (1), 1–14.

[100] Alam, M.S., Saiduzzaman, M., Biswas, A., Ahmed, T., Sultana, A., and Hossain, K.M., 2022, Tuning band gap and enhancing optical functions of $AGeF_3$ (A = K, Rb) under pressure for improved optoelectronic applications, *Sci. Rep.*, 12 (1), 8663.

[101] Penn, D.R., 1962, Wave-number-dependent dielectric function of semiconductors, *Phys. Rev.*, 128 (5), 2093–2097.

[102] Rahaman, M.Z., and Hossain, A.K.M.A., 2018, Effect of metal doping on the visible light absorption, electronic structure and mechanical properties of non-toxic metal halide $CsGeCl_3$, *RSC Adv.*, 8 (58), 33010–33018.

[103] Biswas, A., Alam, M.S., Sultana, A., Ahmed, T., Saiduzzaman, M., and Hossain, K.M., 2021, Effects of Bi and Mn codoping on the physical properties of barium titanate: investigation via DFT method, *Appl. Phys. A: Mater. Sci. Process.*, 127 (12), 939.

[104] Bouhmaidi, S., Pingak, R.K., Azouaoui, A., Harbi, A., Moutaabbid, M., and Setti, L., 2023, *Ab initio* study of structural, elastic, electronic, optical and thermoelectric properties of cubic Ge-based fluoroperovskites $AGeF_3$ (A = K, Rb and Fr), *Solid State Commun.*, 369, 115206.